Applied Catalysis B: Environmental 184 (2016) 119–131

Contents lists available at ScienceDirect

Applied Catalysis B: Environmental

journal homepage: www.elsevier.com/locate/apcatb

TiO_2–SiO_2 films from organic-free colloidal TiO_2 anatase nanoparticles as photocatalyst for removal of volatile organic compounds from indoor air

Andraž Šuligoj[a,1], Urška Lavrenčič Štangar[a], Alenka Ristić[b], Matjaž Mazaj[b], Dejan Verhovšek[c], Nataša Novak Tušar[a,b,*]

[a] Laboratory for Environmental Research, University of Nova Gorica, Vipavska 13, SI-1001 Nova Gorica, Slovenia
[b] Laboratory for Inorganic Chemistry and Technology, National Institute of Chemistry, Hajdrihova 19, SI-1001 Ljubljana, Slovenia
[c] Cinkarna Inc., Kidričeva 26, SI-3001 Celje, Slovenia

ARTICLE INFO

Article history:
Received 4 September 2015
Received in revised form 4 November 2015
Accepted 7 November 2015
Available online 28 November 2015

Keywords:
Photocatalysis
Colloidal TiO_2
TiO_2–SiO_2 Films
Decomposition of volatile organic compounds (VOC)
Indoor air cleaning

ABSTRACT

Different types of TiO_2–SiO_2 composites in the form of powder or films have been reported as efficient photocatalysts for decomposition of organic compounds in liquid and gas phase. Herein, we report for the first time on the formation of efficient TiO_2–SiO_2 films made from acidic organic-free colloidal solution of TiO_2 anatase nanoparticles (AS) and mesoporous SiO_2 (SBA-15) with 100% loading (TiO_2: SiO_2 molar ratio 1:1) under simple and low cost procedure. AS was prepared from metatitanic acid precursor using a novel, environmentally friendly approach of TiO_2 nanoparticles precipitation with NaOH and peptization with HCl. These AS/SBA-15 films, immobilized by brush deposition on glass carriers, showed total decomposition of toluene and 91% decomposition of formaldehyde as model VOCs in gas phase, at room temperature under UVA irradiation in lab-made batch photoreactor. The trend of photocatalytic efficiency for decomposition of formaldehyde was AS/SBA-15 > P25 > PC500 > AS. The adsorption capability of the AS/SBA-15 was higher in comparison to its pure TiO_2 analogues (AS, P25, PC500) in case of toluene. Turnover frequency (TOF) of the AS/SBA-15 was approximately six times higher in comparison to its pure TiO_2 analogue AS for toluene and formaldehyde. The potential of AS/SBA-15 for the use in air cleaning devices is finally discussed.

1. Introduction

Titanium dioxide (TiO_2) is the most used semiconductor for photocatalytic abatement of volatile organic compounds (VOCs) from indoor air due to its interesting characteristics: low cost, safe, high stability, shows high photocatalytic activity, it can promote ambient temperature oxidation of the major class of indoor air pollutants [1–8]. Its activity is based on the absorption of photon of appropriate energy (3.2 eV for anatase), and creation of charge carriers (holes-h^+ and electrons-e^-), thus being active under UV-light. The properties of TiO_2, including its light absorption, charge transfer and surface adsorption, are closely related to its defect disorder, which plays a significant role in the photocatalytic performance of TiO_2 [1]. Among all the defects identified in TiO_2, oxygen vacancy is one of the most important and is supposed to be the prevalent defect in many metal oxides, which has been widely investigated both by theoretical calculations and experimental characterization [1]. The metal doping method (Cr, Mn, Fe, Ni, Cu etc.) [2] or doping with non-metals (N, C, S, F etc.) [3] have been widely used to modify the electronic properties of bulk titania and make TiO_2 effective also under visible light. Another approaches are the combination of TiO_2 and graphene, where sufficient interfacial contact, and in some cases, chemical bonding between semiconductor and graphene enable the extension of the light absorption edge, [9,10] one dimensional structures, where high surface area and short radial distances make possible the absorption of light and low recombination of photogenerated electrons and holes, respectively. [11] Commercial photocatalytic TiO_2 is usually available in the form of powder (examples: Evonik Degussa Aeroxide® P25, Aeroxide® P90, Hombikat UV 100, Millennium PC500, PC50, Kronos KRONOClean 7000, Tipe VPC-10) with excellent activity.

* Corresponding author. Fax: +386 14760300.
E-mail address: natasa.novak.tusar@ki.si (N.N. Tušar).
[1] Present address: Laboratory for Inorganic Chemistry and Technology, National Institute of Chemistry, Hajdrihova 19, SI-1001 Ljubljana, Slovenia.

http://dx.doi.org/10.1016/j.apcatb.2015.11.007
0926-3373/

Colloidal TiO_2 nanoparticles possess compelling benefits of low-cost, large scale solution processing and tuneable optoelectronic properties through controlled synthesis and surface chemistry engineering [4]. These merits make them promising candidates for a variety of applications. TiO_2 colloidal solutions can be prepared with different chemical preciptitation–peptization processes at low temperatures (<100 °C), in which titanium butoxide ($Ti(OBu)_4$), titanium ethoxide ($Ti(OC_2H_5)_4$) or titanium tetraisopropoxide ($Ti(OC_3H_7)_4$) are used as precursors. To avoid the contamination of TiO_2 solutions with organic impurities, titanium tetrachloride ($TiCl_4$), titanium sulphate ($TiOSO_4$) and metatitanic acid (H_2TiO_3) precursor can be used [6,12].

To use TiO_2 in the built-in filter units for air-cleaning devices it has to be deposited on a suitable carrier which are usually honeycomb monoliths. There are several methods available to coat TiO_2 onto material's surface (carriers) as thin film such as dip-coating [13–22], spin-coating [23,24], spraying [25], chemical vapour deposition (CVD) [26] and others. A dip-coating sol–gel method and thermal treatment method are commonly recognized as convenient and practical methods for immobilization of the photocatalytic materials to the carriers due to their simplicity, low cost of operation and tuneable output of the final properties of the materials [27–31]. However, due to the high consumption of the sols, alternatives have also been used, such as brush deposition [32]. Ceramics, glass, metals and other materials have mostly been employed for the manufacture of carriers [27]. Soda lime glass represents a commonly used TiO_2 film carrier even though it contains sodium which has detrimental effect on photoactivity if deposited film is treated at higher temperatures [22,33]. The negative effect of sodium could be eliminated introducing amorphous barrier SiO_2 layer between TiO_2 film and carrier [33,34] or using mixed TiO_2–SiO_2 films [35]. The addition of SiO_2 to TiO_2 also promotes the well-known synergetic effect of both phases: the formation of Si—O—Ti cross-linking bonds and oxygen vacancies in titania [36,37].

A common approach to enhance the photocatalytic activity of TiO_2 is also to increase its surface area (100–200 $m^2\,g^{-1}$ to 400–1000 $m^2\,g^{-1}$). This can be achieved by immobilization of TiO_2 on the porous supports such are porous silica [38–40] or porous carbon [7,8] and the preparation of such a catalyst in the form of thin layer using appropriate carrier. Porous silica (clays, zeolites, mesoporous materials) is superior support for accommodating photocatalysts nanoparticles because they are chemically inert, possess high surface areas, are transparent to UV radiation, have great physical stability, and have hydrophobic character [41–43]. Mesoporous silica SBA-15 [44] with highly ordered hexagonal straight pore arrangement, thick pore walls and high surface area has a lot of advantages if compared to other porous silica supports. It can be prepared over a wide range of pore sizes (5–15 nm) and pore wall thicknesses (3–6 nm) at low temperature (35–100 °C) and possess excellent adsorption properties. In addition to the adjustable silica pore system, strategies for selective immobilization of TiO_2 nanoparticles inside the channels of mesoporous silicas are crucial. The incorporation of photocatalytic active components (TiO_2) in mesoporous silica (e.g. SBA-15, MCM-41) can be achieved by applying different synthesis methods such as wet impregnation [45,46], inner-pore hydrolysis/nonhydrolysis [47–49], co-hydrolysis and co-condensation [50,51], sol–gel processes [52–57] and sol–gel/hydrothermal methods [57]. Among them, the simplest and industrial-friendly are conventional post-synthesis methodologies such as grafting, precipitation or impregnation followed by solvent evaporation [43,47]. However, the vast majority of the studies on titania–silica mixed oxides involve the formation of the active TiO_2 species from titanium alkoxides deposited inside the pores of (ordered) silicas, and attempts in immobilizing the pre-formed TiO_2 nanoparticles inside ordered silica are rare. Adams et al., have encapsulated P-25 titania inside SBA-15 mesoporous thin film silica matrix [58]. Only a small increase in degradation kinetics was found for 20 and 30 wt.% TiO_2 loading compared to 12.5 wt.%, which was ascribed to almost complete absorption of UV light (92%) by the latter sample already. Tobaldi et al., have mixed P-25 with CAB-O-SIL® EH-5 silica with high surface area (380 $m^2\,g^{-1}$) [59]. Oxidation of isopropanol was enhanced upon silica addition and the anatase to rutile transformation was delayed towards higher temperatures. Additionally, the enhancement was ascribed to the more surface hydroxyl groups adsorbed on the photocatalyst surface. Highly cited studies have been published on TiO_2/SBA-15 composites between 2002 and 2006 with TiO_2 loadings up to 80% for decomposition of organic compounds in the liquid phase (photodegradation of organic compounds in water) [53,60–63]. Facet dependent photocatalytic properties of TiO_2-based composites for environmental remediation have been first described by pioneering work of Yang et al. [64] and recently reviewed by Ong et al. [65]. Development of TiO_2-based crystals with small particle sizes and high percentage of exposed {0 0 1} facets remarkably improved photocatalytic performances.

The main emphasis of this work is the evaluation of the photocatalytic efficiency of organic-free acidic colloidal solution of TiO_2 anatase nanoparticles (denoted as AS in this article) in the form of TiO_2–SiO_2 films for the decomposition of toluene and formaldehyde as model VOCs. AS was prepared from metatitanic acid (H_2TiO_3) as a precursor using a novel environmentally friendly approach of TiO_2 nanoparticles precipitation with NaOH and peptization with HCl. Our previous studies for the decomposition of VOCs in the gas phase (photodegradation of VOCs in air) with TiO_2–SiO_2 powders [39,40] or TiO_2–SiO_2 films deposited on the aluminium carriers [66,67] suggest the best performance of the TiO_2–SiO_2 composites with TiO_2: SiO_2 = 1:1 (100% loading). Increasing the titania loading caused an increase in the number of active sites in appropriate places, whereas a further increase of Ti/Si molar ratio led to decrease of the surface area and random dispersion of titania nanoparticles inside the channels of SBA-15 thus narrowing parts of the mesopores of SBA-15. In this respect we developed the low-cost process of immobilization of active TiO_2 nanoparticles of AS into porous silicate support (SBA-15) with high surface area with the molar ratio TiO_2: SiO_2 = 1:1 (100% loading). AS/SBA-15 composite was deposited via brush deposition method in the form of thin layer on glass carriers. Finally, the catalytic activity of AS/SBA-15 composite was compared with AS and also different commercially-available pure TiO_2 (P-25, PC500), used for benchmarking.

2. Experimental section

2.1. Materials preparation

All reagents and solvents for the synthesis and analysis of catalysts were commercially available and used as received without further purification.

Photocatalysts used were the producer-provided commercially-available TiO_2 in powder form P25 (Evonik, Germany), PC500 (Millennium Inorganic Chemicals, USA).

2.1.1. Stable colloidal TiO_2 solution

We developed a novel, environmentally friendly approach for the preparation of colloidal solution of TiO_2 anatase nanoparticles (denoted AS in this article) from metatitanic acid as a precursor using NaOH for precipitation and HCl for peptization. Using this approach we get the same colloidal form of anatase nanoparticles as is possible by adding $BaCl_2$ (aq) [68], because the approach enables the removal of the sulphate bridges that bind the nanopar-

ticles together in the metatitanic acid. The NaOH acts to form the so-called sodium titanate precipitate (Eq. (3)), which is then transformed into nanoparticles by adding HCl (Eq. (4)). We must stress out that the particles in the final colloidal suspension are the same as they are in the starting metatitanic acid, so the method is just a procedure that enables the dispersal of the metatitanic acid agglomerate into individual nanoparticles. The nanoparticles themselves are formed in the process of hydrolysing the dissolved ilmenite in the presence of anatase seeds (Eq. (1)). The conditions of the hydrolysis and especially the amount of the anatase seeds added determine the nanoparticle size and morphology in the metatitanic acid.

$$FeTiO_3 + 2H_2SO_4 \rightarrow TiOSO_4 + FeSO_4 + 2H_2O \quad (1)$$

$$TiOSO_4 + 2H_2O \rightarrow TiO(OH)_2 + H_2SO_4 \quad (2)$$

$$TiO(OH)_2 + 2NaOH \rightarrow Na_2TiO_3 + 2H_2O \quad (3)$$

$$Na_2TiO_3 + 2HCl \rightarrow TiO_2 + H_2O + 2NaCl \quad (4)$$

2.1.2. Mesoporous SiO_2

Ordered mesoporous silica SBA-15 powder was synthesized according to the slightly modified well-known procedure [44]:

8.000 g of Pluronic® P123 triblock copolymer (BASF, Germany) was added to 260.0 mL of distilled water and 40.0 mL of concentrated hydrochloric acid (HCl, 37%, Sigma–Aldrich, USA). The mixture was stirred until the surfactant was dissolved. Next, 17.0 mL of TEOS (98%, Acros Organics) were added while stirring at 45 °C. The reaction gel was stirred for 8 h at 45 °C and aged for another 16 h at 80 °C. The obtained gel with molar ratios of reaction components SiO_2: P123: HCl: H_2O = 1: 0.017: 5.85: 190 was hydrothermally treated in a stainless steel Teflon-lined autoclave at 100 °C for 24 h. The obtained product was continuously washed with distilled water and dried at room temperature. The surfactant was removed by calcination at 550 °C for 6 h in air flow at a heating rate of 1 °C min^{-1}.

2.1.3. TiO_2–SiO_2 composite

To 1.25 mL AS suspension (239.7 g/L) 0.2253 g SBA-15 silica was added and the resulting mixture was diluted with 2.5 mL 1-Propanol (99%, Fluka, Germany). The suspension was afterwards sonicated for 10 min at room temperatures. SBA-15 sample was prepared in the same way, apart from the addition of titania powder.

2.1.4. Titania samples

TiO_2 samples without silica were prepared using the following procedure: AS sample was deposited as prepared. 1 g of P25 TiO_2 powder (Degussa, Germany) was suspended in 7.5 mL absolute ethanol (Sigma–Aldrich, USA). The sample was labelled P25. The suspension was then sonicated for 10 min at room temperature. The same procedure was used for sample PC500, where instead of P25, PC500 TiO_2 powder (Cristal Global, France) was used.

2.1.5. Coating technique

TiO_2–SiO_2 composites and pure TiO_2 samples were additionally stirred during pre-deposition step at 300 rpm at room temperature for half an hour. Then it was sonicated for 10 min at room temperature. It was deposited on glass slides (240 mm × 12 mm × 2 mm) using brush technique, After drying the glass slides with deposited catalyst were heat treated at 150 °C for 1 h. The procedure was repeated until the final mass of 1.0 mg cm^{-2} of the catalyst was obtained. Depending on the sample, this could take from 2 to 5 layers for AS/SBA-15 and AS sample, respectively. The samples were then ready for photocatalytic testing.

2.2. Materials characterization

2.2.1. X-ray powder diffraction (XRD)

XRD patterns were recorded on a PANalytical X'Pert PRO high-resolution diffractometer using CuKα1 radiation (1.5406 Å) in the 2θ range from 5 to 60° (100 s per step of 0.034°) using a fully opened X'Celerator detector. Quantification of phase proportions was done using the method of Spurr and Myers [69] which utilises the ratio of anatase (1 0 1) peak at 25.176° to the rutile (1 1 0) peak at 27.355°. The weight fraction of rutile is therefore given as [70]:

$$w_R = \frac{1}{1 + 0.8\left(I_A/I_R\right)}$$

where, I_A and I_R are the intensities of the anatase (1 0 1) peak and rutile (1 1 0) peak, respectively.

2.2.2. Scanning electron microscopy (SEM)

SEM images were taken using Zeiss Supra 3 VP field emission gun (FEG) microscope, operating at 1 kV. Elemental composition was determined by the energy-dispersive X-ray analysis (EDX) with INCA Energy System, attached to the above-described microscope, operating at 20 kV.

2.2.3. High-resolution transmission electron microscopy (HRTEM)

HRTEM was performed on a 200 kV field-emission gun (FEG) microscope JEOL JEM 2100. For HRTEM studies a drop of an ethanol diluted nanoparticles solution was placed on a copper grid and dried at room temperature. The specimens were additionally coated with carbon in order to prevent excessive charging and decomposition of the sample under the electron beam.

2.2.4. N_2-physisorption

Nitrogen adsorption measurements were measured at 77 K on a Tristar 3000 Micromeritics volumetric adsorption analyser. Before the adsorption analysis, the samples were outgassed under vacuum for 2 h at 473 K in the port of the adsorption analyzer. The BET specific surface area [71] was calculated from adsorption data in the relative pressure range from 0.05 to 0.25. The total pore volume was estimated on the basis of the amount adsorbed at a relative pressure of 0.97 [72]. The pore size distributions (PSDs) were calculated from nitrogen adsorption data using a BJH algorithm based on ideas of Barrett et al., [73]. The maxima on the PSD are considered as the primary mesopore diameters for given samples.

2.2.5. Fourier transform infrared spectroscopy (FT-IR)

The FT-IR spectra were collected on a Perkin Elmer Spectrum 100 spectrometer, using a KBr pellet method. 2 mg of sample was grinded in mortar with 200 mg potassium bromide. Spectra were collected from 4000 to 450 cm^{-1} and processed using Spectrum 6.3.5 software.

2.2.6. UV–vis diffuse reflectance spectroscopy (DRS)

DRS measurements were made using LAMBDA 650 UV/Vis with PerkinElmer UV WinLab 6.03 software. The band-gap energies were determined using the following equation [74]:

$$E_g\,(eV) = \frac{1239.8}{\lambda}$$

where λ is the absorption edge and E_g is the band-gap energy

2.2.7. Elemental analysis

The concentration of titania present in the composite sample was determined with Inductively coupled plasma atomic emission spectroscopy (ICP-OES) on Varian 715-ES.

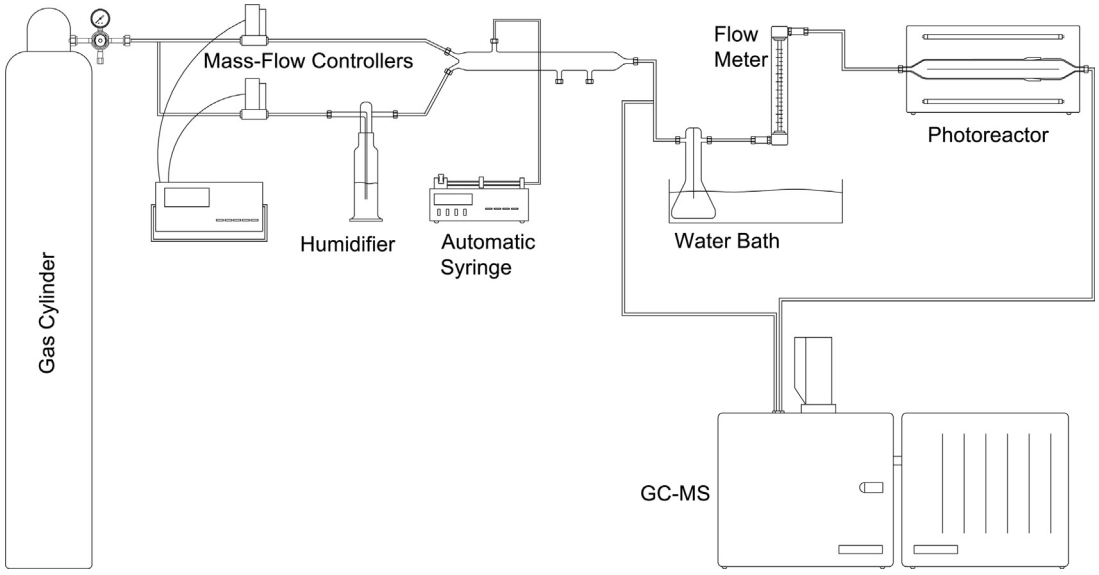

Fig. 1. Experimental set up scheme.

2.3. Photocatalytic tests

Photocatalytic properties of the catalysts were measured with the oxidation of toluene in a lab-made batch photoreactor system (Fig. 1) [66]. The volume of the system is 2.0 L and the flow is set to 400 mL min^{-1}. The system consists of synthetic air cylinders, humidifier and a mixing chamber where the pollutant is introduced into the system. When enough testing molecule is injected to the system, the path from the mixing chamber to other parts of the system is closed and the set-up is put in batch mode. An on-line port for taking the gas samples directly to the GC–MS apparatus is set after the Rayonet photoreactor, equipped with up to 14 UV or visible lamps. The concentration of toluene was determined with Saturn 2100T gas chromatograph from Varian. The column (Varian CP-Porabond U, 0.32 mm ID, 25 m) in the GC–MS apparatus was set at 80 °C and was heated to 180 °C at a rate of 10 °C min^{-1}, where it was held for 2 min. Finally, it was cooled down to 80 °C at a rate of 100 °C min^{-1}. The injector was set to split mode with a ratio of 10. The mass range in the mass spectrometer was set to 15–50 m/z for the first 3 min, for better sensitivity when detecting CO_2, but was then adjusted to 15–150 m/z. The irradiation power of the light source (two lamps opposite to each other) was 3.64 mW/cm^2 (Philips Cleo 15 W with broad maximum at 365 nm). The first model compound chosen was toluene with an initial concentration of 49.0 ± 2.4 ppmv. The quantification of carbon dioxide was carried out by calibration for CO_2 with a 10 L gas bottle, containing 500 ppmv CO_2 in nitrogen. In each experiment one glass slide was used which equalled to approximately 65 mg of catalyst. Each experiment was conducted three times using a fresh catalyst from the same batch to obtain standard deviations (SD).

Reaction rates were calculated using the following equation:

$$\ln\left(\frac{c_0}{c}\right) = k \times t$$

where, c_0 is the concentration before the ignition of the lamps, c is the concentration at time t, and k is the reaction rate constant obtained from the plot of $\ln(c_0/c)$ versus time (t).

The second photocatalytic test was done in the same manner as the aforementioned, with the change of the model compound to formaldehyde. The initial concentration was set to 3.0 ± 0.1 ppmv. The quantification of the pollutant was carried out with HALHFX205 formaldehyde meter, with a calibration range 0–10 ppmv and a resolution of 0.01 ppmv (Hal Technology, USA).

Turnover frequencies (TOF) were also determined. The total amount of toluene degraded in all tests (total degradation) was 4.03×10^{-6} mol = 2.46×10^{18} molecules. However, because the calculating an "average" TOF at high reactant consumption underestimates the initial instantaneous TOF [75] and because the adsorptions of some materials were very high, the determination of TOF times at 40% degradation were used, giving number of toluene molecules 1.48×10^{18}. The amounts of titania used in the tests with pure TiO_2 samples were 65 mg, whereas the weight of TiO_2 in AS/SBA-15 sample was determined with ICP-OES. To estimate the number of active species value 5×10^{14} a.s. cm^{-2} was used [76]. Hence the TOF was calculated as:

$$\mathrm{TOF} = \frac{1.48 \times 10^{18}/5 \times 10^{14} S_{BET} \times m(TiO_2)}{t}$$

where S_{BET} is the surface area of TiO_2 determined by N_2-physisorption in m^2g^{-1}, $m(TiO_2)$ is the weight of titania used in reaction in g and t is time needed for a sample to reach 40% degradation of the model pollutant in s.

3. Results and discussion

3.1. Preparation of photocatalysts

A stable acidic colloidal solution of TiO_2 anatase nanoparticles (AS) was prepared from metatitanic acid with very low pH value (pH 1.1) and small TiO_2 aggregates around 50 nm in size. The aggregates are formed from TiO_2 crystallites approximately 5–10 nm in size (see descriptions of XRD Fig. 2 and TEM Fig. 4) make AS an ideal impregnation material for the silica support. TiO_2–SiO_2 composite films made from AS and mesoporous SiO_2 (SBA-15) with 100% loading (TiO_2: SiO_2 molar ratio 1:1) were prepared under simple procedure, which involved wet chemistry and low-temperature immobilization under ambient pressure (see Section 2.1). In order to assess the properties and photocatalytic activity of this material a comparison to commercial benchmark materials was carried out.

Commercial pure titania P-25 is a well-known benchmark material, used for photocatalytic decomposition of organic compounds in water and air, mainly due to its specific anatase to rutile ratio (78% anatase, 14% rutile and 8% amorphous phase [77]) and its

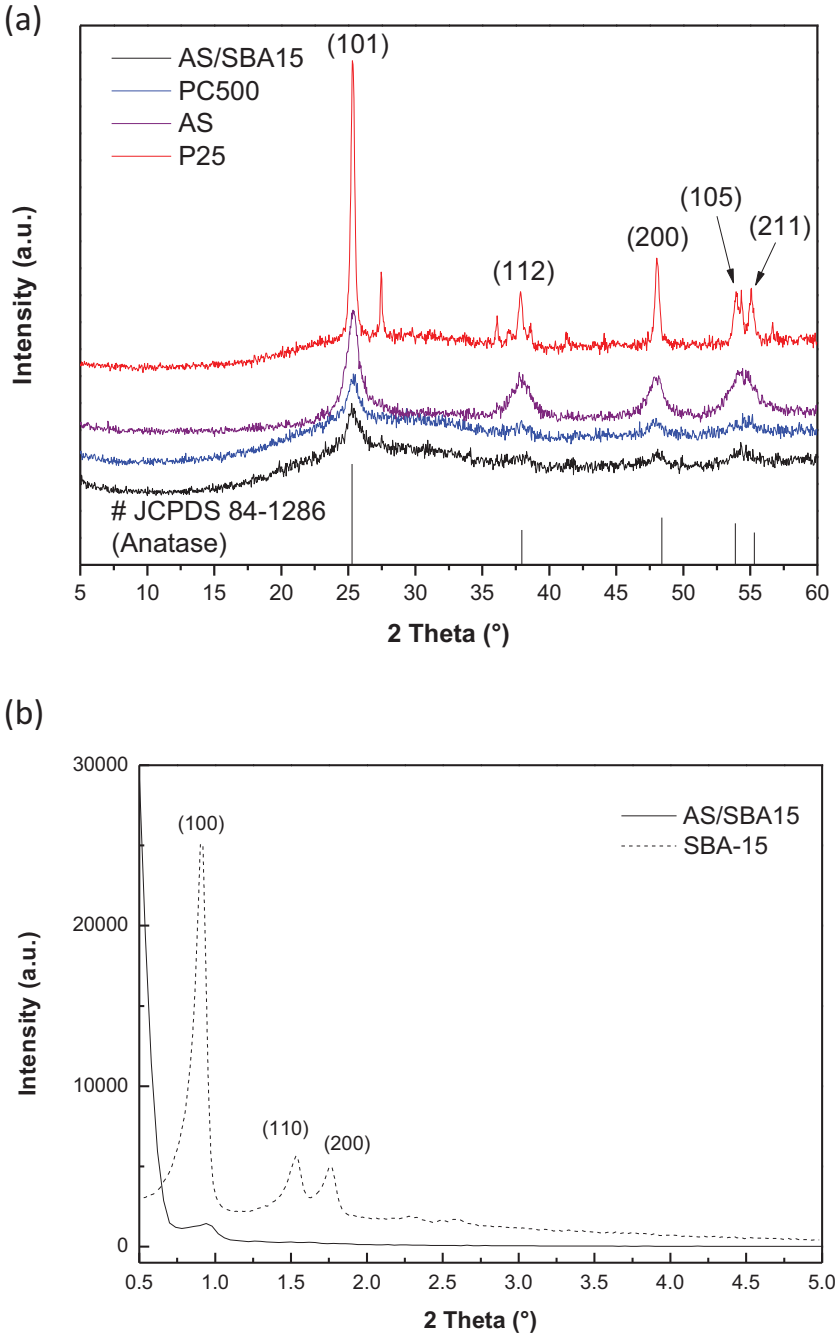

Fig. 2. (a) Wide-angle XRD patterns of P25, PC500, AS. Atomic planes for anatase are labeled. (b) Low-angle patterns of silica support (dashed line) and the TiO_2–SiO_2 composite (solid line).

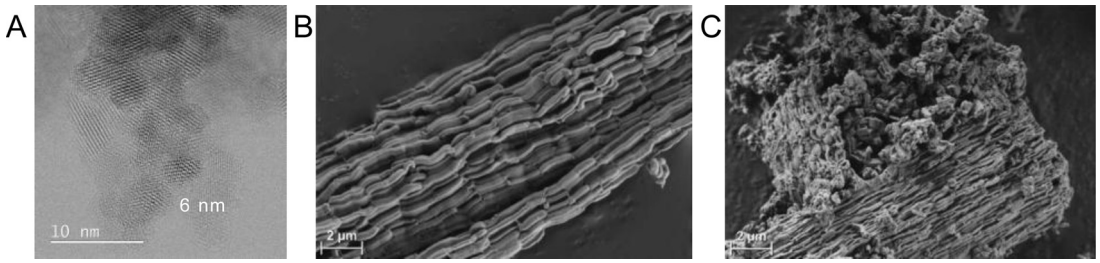

Fig. 3. (a) TEM micrograph of AS TiO_2 with the size of nanocrystals labelled. SEM micrographs of (b) SBA-15 support and (c) AS/SBA-15 composite.

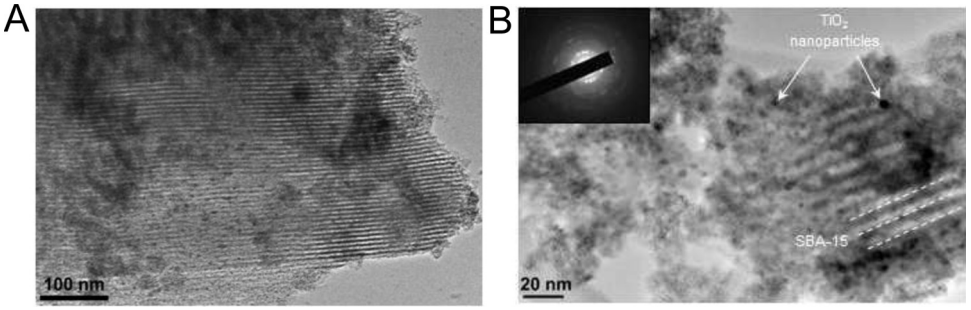

Fig. 4. (a) Typical TEM micrograph with large degree of SBA-15 mesostructure disorder. (b) TEM micrograph revealing anatase TiO_2 nanoparticles within mesoporous silica matrix in sample AS/SBA-15. Inset on the upper left side shows electron diffraction performed on the corresponding area (SAED).

Table 1
Structural parameters of materials.

Sample	S_{BET} (m^2/g)[a]	V_{tot} (cm^3/g)[a]	Pore size (nm)[a]	Crystal size (nm)[b]	Band gap (eV)[c]
SBA-15	855	1.227	9.2	–	/
AS/SBA-15	460	0.711	6.3[d], 9.3, 18.2	8.6	3.16
AS	291	0.368	2.2	11.4	3.02
P25	47	/	2.5	25.8	3.03
PC500	276	0.276	2.1	12.9	3.14

[a] S_{BET}, V_{tot} and pore sizes determined by N_2-sorption isotherms.
[b] Crystal size determined by Scherrer equation from the XRD data for the largest anatase (1 0 1) peak at 25.1°.
[c] Band gaps determined from UV–vis diffuse reflectance spectra.
[d] Shoulder.

high water dispersion and stability. However, since the size of P-25 nanoparticles is around 25 nm, they are too large for their incorporation into the pores of SBA-15 (cca. 9 nm). Hence, pure P-25 catalyst was used as a reference. On the other hand, commercial PC500 is a pure anatase-phase titania, with high surface area (Table 1), making it an ideal commercial reference to AS (pure anatase-phase titania), which has even higher surface area but similar pore sizes (Table 1). Hence, it was used as a second reference photocatalyst.

3.2. Physico–chemical properties of photocatalysts

3.2.1. XRD

High-angle XRD patterns (Fig. 2a) of commercial TiO_2 materials P25, PC500 and AS show that PC500 and AS consist of pure anatase crystalline phase. The XRD analysis of P25 indicated the presence of anatase (JCPDS 84-1286) and rutile phase (JCPDS 4-0551). The final quantitative analysis resulted in composition of 82% of anatase and 18% of rutile with the crystallites size of 10 nm and 3 nm, respectively. The higher content of rutile found (18%) if compared to commercial data (14%) is not new as it is well known that fluctuation in P25 crystal phase content is attributable to inhomogeneity of the crystal composition of P25 [77]. Particle sizes were calculated from the Scherrer equation for all 3 samples (Table 1) from the most intense diffraction peak (1 0 1) corresponding to peak at 2θ 25.31°, and coincided to information specified from the producers. The low crystallinity of PC500 sample can be observed from the low intensity of (1 0 1), (1 1 2), (2 0 0) and (1 0 5) anatase diffraction peaks due to a significant fraction of amorphous material (20–25%) also seen in the hump at 15–35°. On the other hand, AS titania showed good crystallinity at all major 2θ positions for anatase phase. A strong reduction in diffraction line intensity of anatase is seen in sample AS/SBA-15. This does not reflect the degradation/transformation of the anatase phase but is rather a result of X-Ray diffractions of additional guest phase of SBA-15 thus reducing the TiO_2 concentration in the mixture. The hump at 15–35° 2θ positions in this sample is a consequence of signal from amorphous silica (SBA-15).

Low-angle XRD patterns of SBA-15 and composite AS/SBA15 are visible in Fig 2b. The patterns of pure silica exhibited a very intense peak at 2θ = 0,92°, together with two other weak peaks between 1.53° and 1.77°, which correspond to the (1 0 0), (1 1 0), and (2 0 0) planes in a hexagonal arrangement, respectively. Upon impregnation, the diffraction peaks at 1.53° and 1.77° disappeared and the peak representative for (1 0 0) plane was greatly reduced, which demonstrated the partial collapse of the ordered structure of SBA-15.

3.2.2. Electron microscopy

STEM image Fig. 3a shows that AS comprises of a single phase anatase (previously confirmed by XRD) and consists of crystals with their size ranging 6–10 nm. In Fig. 3b SBA-15 shows typical hexagonal morphology while in Fig. 3c AS/SBA-15 composite clearly shows two phases—TiO_2 and SBA-15. Moreover, a partial destruction of the SBA-15 structure is visible upon impregnation with TiO_2 (Fig. 3c), which coincides well with the low-angle XRD measurements. Titania nanoparticles are located also inside the collapsed SBA-15 structure, which could cause some pore blockings (vide infra).

The TEM micrograph shown in Fig. 4a indicates mesostructured nature of the sample with 1-dimensional parallel mesoporous channels typical for SBA-15-type material. However, more thorough TEM observations show that most of the sample possesses low degree of the mesostructure integrity. Micrograph shown in Fig. 4b reveals the presence of TiO_2 nanoparticles with the estimated size of 5–10 nm which seem to be located within the mesopores of the silica matrix. The nanoparticles become more visible in slightly overfocussed bright image conditions, where the contrast between the areas corresponding to silica matrix and titania nanoparticles is enhanced (Fig. 4b). The selected area electron diffraction (SAED) shown on the inset of the Fig. 4b confirms the polycrystalline nature of the TiO_2 nanoparticles in anatase form.

3.2.3. N_2-physisorption

Gas physisorption is extensively used in the characterisation of porous solids, particularly for evaluation of their specific surface

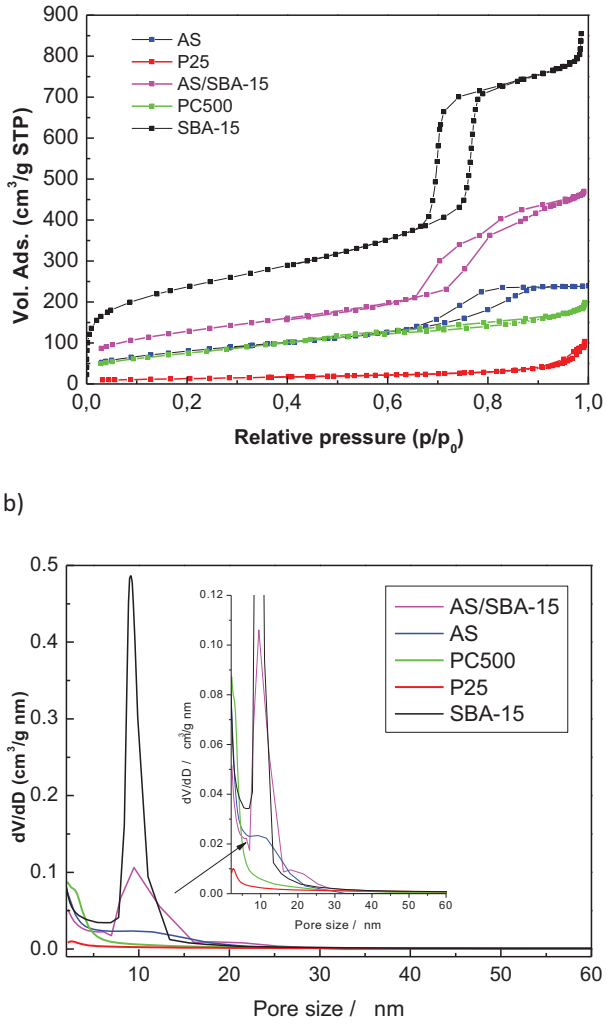

Fig. 5. (a) Nitrogen sorption isotherms of SBA-15, AS/SBA-15, AS, P25 and PC500, (b) pore size distribution of SBA-15, AS/SBA-15, AS, P25 and PC500. (inset: enlarged graph of PSD).

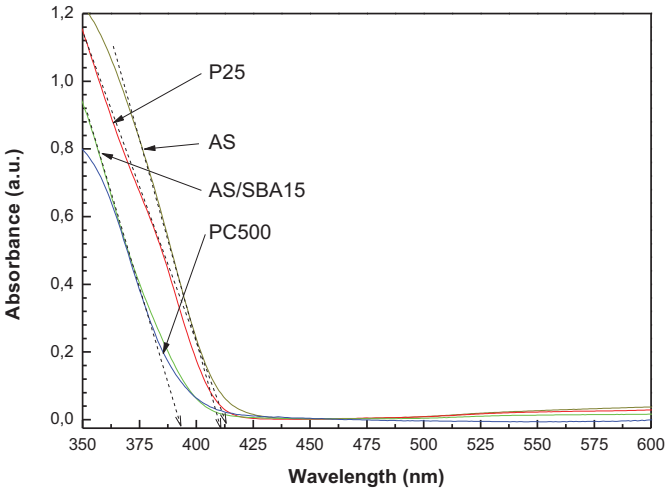

Fig. 6. UV–vis diffuse reflectance measurements of the catalysts.

area, total pore volume, pore size distribution as well as surface properties. The shape of the isotherm obtained from these adsorption measurements is very important as it can reveal the kind of porosity (micro-, meso- or macroporosity) present in the sample. Nitrogen adsorption isotherms for materials are shown in Fig. 5a, whereas pore size distributions are indicated in Fig. 5b, together with the inset showing detailed part of PSD of AS/SBA-15. Structural parameters determined on the basis of these isotherms are listed in Table 1. The difference of isotherms types and hysteresis loops can clearly be seen in Fig. 5a. Samples SBA-15, AS/SBA-15, AS and PC500 exhibit type IV sorption isotherms, while sample P25 shows isotherm type II [72]. SBA-15 sample exhibits sorption isotherm with relatively narrow hysteresis loop of H1 type, typical for ordered mesoporous silicas with hexagonal pore arrangement [72]. Additional hysteresis loop at relative pressure above 0.97 on sorption isotherm is present in this sample, evidencing the presence of an interparticle or textural porosity [78]. It can clearly be observed that AS titania impregnation of SBA-15 (AS/SBA-15) leads to a marked change in the shape of the hysteresis loop, showing on partial collapse of ordered pore arrangement into disordered pore arrangement, which finds some evidence in SEM, TEM and XRD analyses. Besides that, the hysteresis loop of this sample is closing down at lower P/P_0 value in comparison to the original support, which indicates that pores are partially narrowed with titania nanoparticles. The loading of titania nanoparticles into SBA-15 support led to a decreased specific surface area, pore volume and multimodal porosity (Table 1). It can be concluded that titania nanoparticles have been dispersed inside of the support, which is in agreement with TEM. Furthermore, titania nanoparticles are present also on the external surface of the support, which is evident by the decrease of the textural porosity due to TiO_2 nanoparticles filling of the voids between SBA-15 particles. For AS sample, titania nanoparticles are less uniform and their agglomeration leads to irregular mesoporous structure with broader pore size distribution. The latter is reflected by H2 hysteresis, often attributed to porous inorganic oxides [79]. Sorption isotherms of samples P25 and PC500 indicate the presence of mesopores [72]. Pore size distribution (Fig. 5b) of the different mesoporous materials has been determined using the BJH model widely used for this type of samples [73,80]. Although this model often underestimates pore sizes, it is appropriate for comparative purposes [81]. The pore size distribution determined from adsorption isotherms shows one distinguished maximum for SBA-15, AS and P25, while for AS/SBA-15 two maxima with a shoulder are present, indicating on the existence of partly narrowed mesopores with titania. PC500 exhibits very broad pore size distribution with no apparent maximum, due to the technique limits of the nitrogen adsorption-desorption apparatus [78].

3.2.4. DRS

UV–vis diffuse reflectance spectra shown in Fig. 6 indicate an increase in band-gap energy (E_g) of titania in the case of SBA-15 impregnation with AS titania. A number of studies have linked higher band-gap values to decreased number of surface defects in titania nanocrystals [82–84]. These defects are probably in the form of oxygen vacancy or Ti^{3+} defects, as these have been found to be the main source of defect states in titania [84]. On the other hand, increased band gap can be associated with well-known quantum size effect [85]. The increase in our case (see Table 1, AS/SBA-15) is probably a result of both phenomena. Hence, the increased energy band-gap could result in the lower recombination of the charge carriers (h^+ and e^-) and higher oxidative potential, which would be beneficial for the photocatalytic process. Interestingly, the band-gap value of AS/SBA-15 is very similar as in the PC500 sample which contains amorphous phase, and it is known that amorphous materials show higher band-gap values, even exceeding 3.5 eV [86].

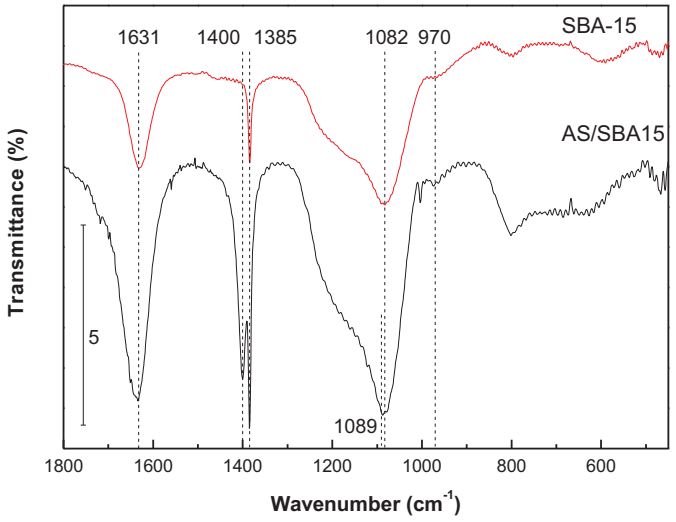

Fig. 7. FT-IR spectra of pure (SBA-15) and grafted mesoporous silica (AS/SBA-15).

3.2.5. FT-IR

FT-IR spectra of the samples are shown in Fig. 7. A strong band at 1089 cm^{-1} present in AS/SBA-15 sample belongs to asymmetric stretching of Si—O—Si bonds, whereas the band at 970 cm^{-1} is attributed to Ti—OH stretching vibration. However, upon impregnation with TiO_2, the relative intensity of this peak compared to the peak at 1982 cm^{-1} (Si—O—Si) decreases, indicating that the impregnation method did not result in covalent bonds [87,88] between titania and silica, i.e., TiO_2–SiO_2 mixed oxide, but rather in Van der Waals attraction forces binding the TiO_2 nanoparticles into the framework of SBA-15. Moreover, the peaks position stayed the same, whereas in case of mixed oxides usually a slight shift to lower frequencies should occur [89]. The peak at 1631 cm^{-1} corresponds to the OH bending vibrations of the surface Si—OH and Ti—OH groups in mesoporous materials, and has a relatively higher intensity compared to 1082 cm^{-1} peak in case of AS/SBA-15 sample and is a consequence of the contribution of Ti—OH groups present on TiO_2. The broad absorption peak appearing around 3440 cm^{-1} is attributed to the stretching mode of the O—H bond of the surface adsorbed water and hydroxyl groups [90], whereas the peak at 1400 cm^{-1} is attributed to Ti—O—Ti vibration, present only in AS/SBA-15 sample. Hence, these results further support the conclusion that TiO_2 was impregnated not only in SBA-15 mesopores, as this would result in higher Ti—Si interaction [89], but also outside the mesoporous silica as a separate phase, which was also evident in the TEM images (Fig 4b).

3.3. Activity tests of photocatalysts

3.3.1. Photocatalysis of gas-phase toluene

Decomposition of toluene is shown in Fig. 8 and followed apparent first-order exponential decay (Fig. 8b). Toluene decomposition was not observed in the absence of TiO_2 catalyst, i.e., in the blank sample (Fig. 8), therefore all variations in the concentrations of the pollutants during illumination period were prescribed to photocatalytic activity of the catalysts. Oxidation was complete (total decomposition) for all the samples in the given experimental timeframe (5 h), apart from sample AS, where the final concentration of CO_2 reached 65.8% of total stoichiometric amount. However, even with this sample, no toluene was found in the reaction system at the end of the experiments, nor were there any intermediates detected in the gas phase. The low CO_2 production in AS sample together with fast kinetics means the catalyst is generating the charge carriers efficiently, for the decomposition of toluene. However, it seems

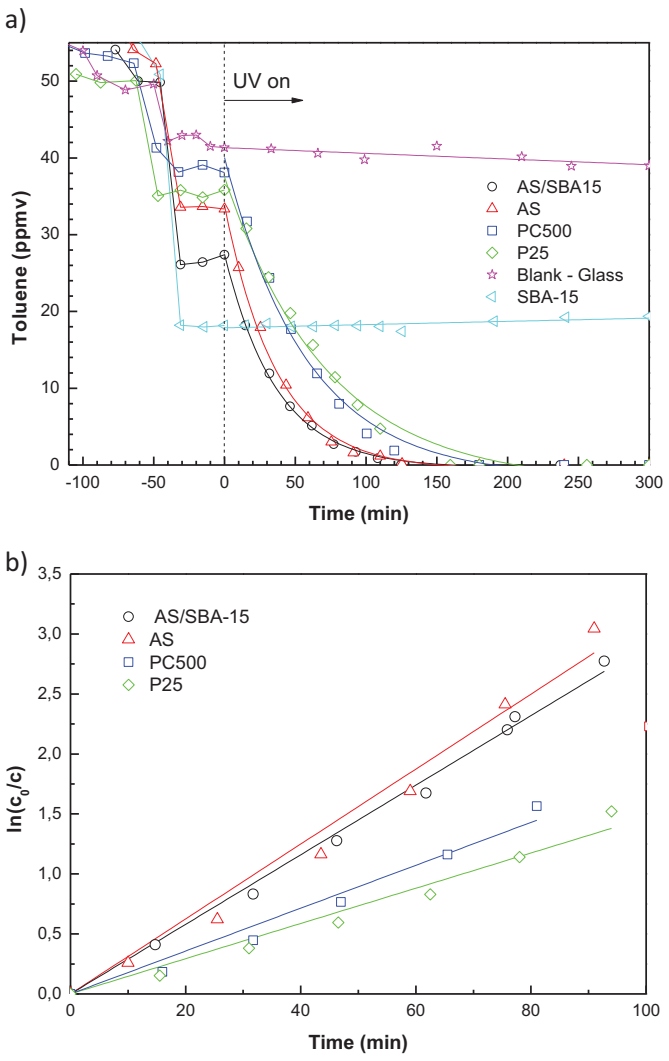

Fig. 8. (a) Photocatalytic degradation of toluene in the presence of the catalysts, pure SBA-15 silica and glass slide blank. (b) Semilog transformation to test the first-order reaction rate.

that intermediates in the degradation pathway are stable and also having low vapour pressure. On the other hand, this problem could be addressed in an air cleaning device by employing the cleaning mode of operation. This means that catalyst would be exposed to clean air while still irradiating with UV light [91].

However, one possible reason for the less-than-complete oxidation in the case of AS sample lies in its relatively low band gap value (3.02 eV, see Table 1), suggesting a higher number of structural defects compared to other samples or larger nanoparticles. The latter was dismissed with N_2-physisorption and evaluation of the crystal size by XRD (Table 1). Because the surface area of the sample is large enough and the irregular pore size distribution permits fast adsorption of toluene this resulted in high reaction rate constant. As can be observed from Fig. 8b, the kinetics of AS was almost twice faster than PC500 sample, which coincides nicely with higher surface area of the former sample. In accordance with this was the kinetics of AS/SBA-15 sample which was faster than TiO_2 sources, appart from AS TiO_2 (Table 2).

To further elucidate the role of surface area of the catalysts TOFs were calculated (Table 2). The amount of Ti in AS/SBA-15 sample was determined with ICP-OES to be 28.45% (m/m), hence the weight fraction of TiO_2 being 0.475, which is in agreement with the TiO_2: SiO_2 molar ratio in the preparation procedure. It must be

Table 2
Photocatalytic features of the samples for the decomposition of toluene.

Catalyst	Rate constant $\times 10^{-3}$ (min^{-1})	R^2	TOF $\times 10^{-5}$ (s^{-1})	Adsorption (%)	CO_2 yield (%)
P25	14.7 ± 1.6	0.989	5.65	12.6	97.5
PC500	17.9 ± 1.4	0.989	1.01	7.1	96.8
AS	31.2 ± 0.2	0.992	2.21	18.6	65.8
AS/SBA-15	29.0 ± 1.1	0.998	13.1	33.2	97.0

noted that the amount of TiO_2 present in the composite in this research is high, as other researchers have claimed that excess amount of titania inside the pores results in pores being blocked hence decreasing the performance of the composites [6]. We can observe that in the pure materials, P25 actually showed the highest TOF (2.5 times higher than AS). When the AS catalyst was grafted into SBA-15 its turnover frequency was improved almost six times to $1.31 \times 10^{-4}\ s^{-1}$. The increased value of TOF is mainly the consequence of improved adsorption, hence providing the pollutant to the active site more efficiently. This clearly shows on the important role of mesoporous silica on the activity of catalysts.

However, other factors must not be underestimated. As expected, large E_g value resulted in complete oxidation of the model molecule, due to high oxidation potential. Therefore, the kinetics of decomposition of toluene, showed a trend AS > AS/SBA-15 > PC500 > P25. Similar trend was evident also in the time needed for concentration of the pollutant to reach zero (Fig. 8a). Regarding the adsorption of toluene, it was 26.80% for AS/SBA-15 sample, due to its high surface area [40], whereas for pure titania samples, the adsorption of toluene was much lower (below 10%) and was the lowest in the samples P25 and PC500. Therefore, it can be concluded that toluene decomposition depended not only on the surface area of the photocatalyst, but also on its crystal size (Table 1). As the surface area of the catalyst was increased, the photocatalytic activity increased as well due to the increased number of adsorption sites and hence increased adsorption. Small titania particles or small aggregates within SBA-15 support (Fig. 4b) additionally contribute to higher decomposition rate constant of AS/SBA-15 (Table 2). The fact that the structure of SBA-15 was partially ruined did not result in decreased adsorption and/or photocatalytic properties, hence the use of acidic colloidal form of TiO_2 for the impregnation of ordered mesoporous silica has been proven purposeful.

Samples used in this study were in 5–20 μm thick, which is sufficient to absorb all the incident photons. It has been shown [92] that toluene removal efficiency increased with the TiO_2 thickness (i.e., mass) until a maximum value of 500 nm, beyond which the removal efficiency did not increase further under UVA and UVC light irradiation. However, samples used in this study can be defined as thick, and in this case, the limiting parameter is the diffusivity of the pollutants in the films. Therefore in the case of AS/SBA-15, the porosity of the sample is allowing the molecules of toluene and formaldehyde to reach the active sites and be decomposed. Because light absorption depends on the mass of titania and not on the layer thickness (in the case of TiO_2–SiO_2 composites), this means that the optical distance for films with lower and higher porosity is the same. This is the case in AS/SBA-15 where pore volume was almost doubled ($0.711\ cm^3\ g^{-1}$) compared to AS ($0.368\ cm^3\ g^{-1}$, Table 1), mass of TiO_2 was halved while reaction rate constant remained practically the same. It is then reasonable to conclude that titania nanoparticles were adequately irradiated, thus resulting in high photocatalytic efficiency. The UV photon flux (Φ) which is irradiating the catalyst has an influence on the reaction rate defined as:

$$r = r' \Phi^{m}$$

where r' is the reaction rate independent of the photon flux and m is related to the efficiency of electron–hole formation. The photon flux used in this study surpasses the value of 1–2 $mW\ cm^{-2}$ up to which the r linearly ($m = 1$) increases with increased Φ [17]. Because AS is 100% anatase this means that under these conditions the electron-hole recombination is the dominant process on the surface. This process is dominated by the presence of structural defects, hence they should be considered.

Related to the principles of photocatalysis, the encapsulation of TiO_2 in SiO_2 improved crystallinity of titania. This has been characterized by lower number of structural defects, which can act as recombination sites for the generated charge carriers, hence decreasing their lifetime and lowering the rate of electron–hole couple generation per incident photon (quantum efficiency). As it is known that toluene adsorbs on the surface Ti—OH as well as Si—OH groups via OH—π electron-type interaction [93], the fast degradation in sample AS/SBA-15 is a strong indication that toluene molecules adsorb on surface titanol groups and not only silanol ones, as that would result in high disappearance of toluene but not complete decomposition to CO_2 as is the case here. On the other hand, this could also mean, that toluene adsorbs primarily on Si—OH groups close to active sites, i.e., TiO_2, since titania nanoparticles were located inside as well as outside the SBA-15 pores (see Sections 3.2.3 and 3.2.5)

3.3.2. Photocatalysis of gas-phase formaldehyde

The decomposition of formaldehyde was the fastest with PC500 titania followed by P25 and AS/SBA-15 sample (Fig. 9). It must be noted, that the determination of k for this sample was rather difficult due to few initial measurement points that followed the first-order kinetics. However, PC500 photocatalyst contains mesopores of 2.1 nm (Table 1), which can give access to small (gaseous) pollutants. Therefore, as the diameters of formaldehyde and toluene are 0.24 nm and 0.67 nm, respectively [94] the small size of pores acts beneficial for the adsorption of formaldehyde molecule. Interestingly, the adsorption of formaldehyde onto PC500 sample was even greater than in case of SBA-15, confirming the importance of small pore sizes (Table 1). However, this does not have a direct correlation with the decomposition efficiency since it was in the order of AS/SBA-15 > P25 > PC500 > AS, but without any big differences among various titania samples. In the case of AS/SBA-15 sample, the addition of the mesoporous silica improved the adsorption of the model molecule remarkably, i.e. from 7.6% to 38.0%. The TOF values show (Table 3) the highest activity of P25 sample, which in spite of having the lowest adsorption showed high TOF and rate constant. On the other hand, due to very high adsorption PC500 sample TOF at 40% degradation was not calculated. However, total decomposition of formaldehyde was not reached with any sample and the highest decomposition efficiency was achieved by the sample AS/SBA-15 (91.3%). The trend of efficiency for decomposition of formaldehyde was found to be AS/SBA-15 > P25 > PC500 > AS. Other researchers have shown [95,96] that TiO_2 photocatalysts were able to decompose formaldehyde to a certain degree, whereas the 10 wt.% addition of other metal oxides i.e. CrO_2, WO_3, MnO_3, ZnO generally decreased the decomposition efficiency, with the exception of SiO_2 where the efficiency was increased up to 94% [95,96], which is in accordance with our results. The phenomena could be explained by taking into account the band gap values of the catalysts. Although PC500 exhib-

Table 3
Photocatalytic features of the samples for the decomposition of formaldehyde.

Catalyst	Rate constant × 10^{-3} (min^{-1})	R^2	TOF × 10^{-6} (s^{-1})	Adsorption (%)	Degradation efficiency (%)
P25	66.2 ± 6.4	0.959	21.2	9.8	90.7
PC500	139.1 ± 18.2	0.996	–	75.6	90.6
AS	34.9 ± 4.0	0.996	1.13	10.3	88.3
AS/SBA-15	37.9 ± 3.8	0.957	6.17	37.1	91.7

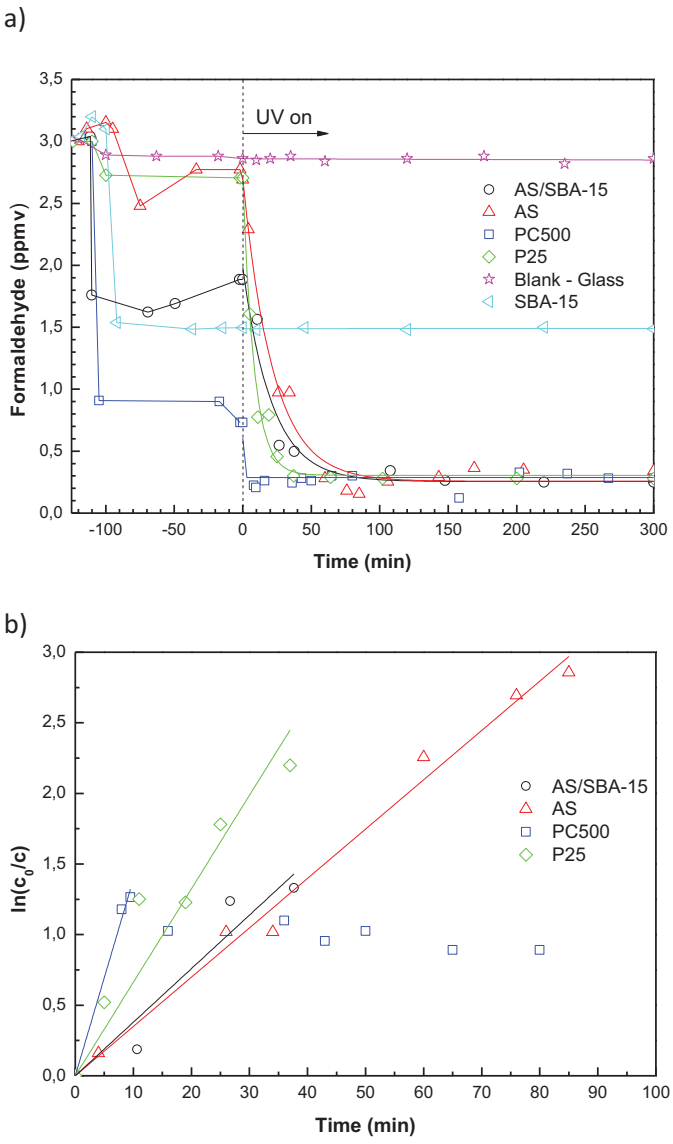

Fig. 9. (a) Photocatalytic degradation of formaldehyde in the presence of the catalysts, pure SBA-15 silica and glass slide blank. (b) Semilog transformation to test the first-order reaction rate.

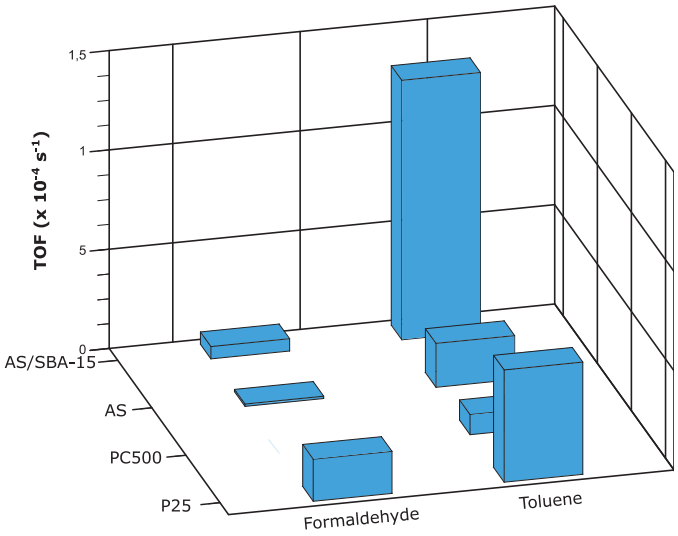

Fig. 10. TOF values of formaldehyde and toluene in the presence of the catalysts.

ited high E_g total decomposition of formaldehyde was not reached, hence this confirms the claim, that high E_g value in this sample is partly a consequence of the presence of amorphous phase of titania. On the other hand, the decomposition efficiency of AS was improved from 87,9% to 91,3% when grafted to SBA-15, which is a consequence of improved crystallinity (Fig. 6) and good access of the model molecule to catalytic sites, as discussed above.

To sum up the results of the photocatalytic testing together with characterization methods, the following trends can be observed.

From Fig. 10 it can be seen, that the catalysts were approximately 20 times more active in case of toluene degradation compared to formaldehyde, which is in accordance with other researches [97]. The exception is P25 where toluene degradation was only 2.67 times faster. However, Adams et al. [58] have grafted P25 into SBA-15 pores and found only little improvement in photoactivity between 12.5% and 30% TiO_2 loading onto SBA-15. The enhancement (regarding TOF) of AS TiO_2 activity upon grafting to SBA-15 found in this research was 5.5 and 6 times in formaldehyde and toluene oxidation, respectively. Additionally, this shows that silica improves the activity of the surface active sites (TOF takes into account the number of these) and/or improves the structure of the surface of the catalyst. On the other hand, DRS measurements have shown (Fig. 6) a change in bulk lattice structure and size of nanocrystals, hence the increased band gap upon the addition of silica. Ordered silica thus serves as a surface structure-directing agent and it alters the bulk lattice properties [98].

Therefore, the distribution of AS titania nanoparticles in/on SBA-15 affected the accessibility of the active sites to the pollutant, hence improved the degradation kinetics. On the other hand, higher crystallinity of AS titania nanoparticles in/on SBA-15 prolonged the lifetime of charge carriers, hence improving the efficiency of the reaction. Hence, titania in colloidal form, with size of nanoparticles small enough to be encapsulated into mesopores of silica is appropriate for the impregnation of such SiO_2. Accordingly, the sample AS/SBA-15 has proven to be the most suitable for toluene as well as formaldehyde decomposition and the addition of mesoporous silica SBA-15 is a purposeful way of improving the properties of photocatalytic materials.

Long term use of the composite catalyst towards toluene oxidation is presented in Fig. 11. In comparison to pure titania i.e., AS, the composite shows similar loss of activity during three consecutive runs. However, the adsorption capacity only decreased by little less than 3% (from 33.2 to 30.6%) in the third run in AS/SBA15 sample, whereas this difference was higher (from 18.6 to 11.3%) in AS sample. On the other hand, the samples were not cleaned during the consecutive runs, hence this difference in adsorption capacity is probably the consequence of longer exposure to cleaned air in

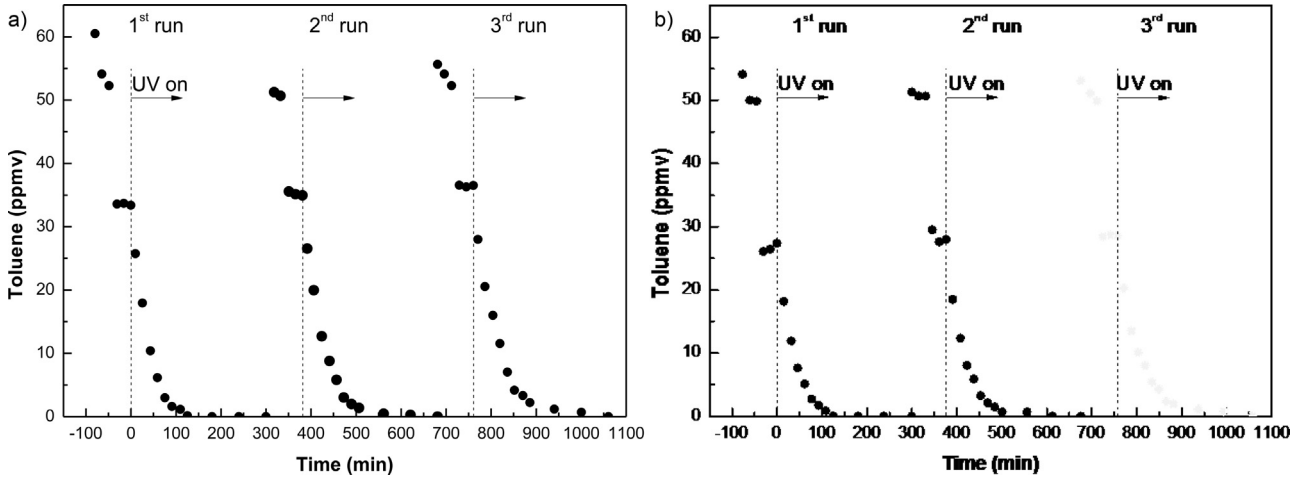

Fig. 11. Recycling experiments with samples (a) AS and (b) AS/SBA15.

case of AS/SBA15, i.e., the polluted stream was cleaned in 240 min in 3rd run, while comparable air cleanness was reached in 300 min when sample AS was used. Hence, the composite sample had more time to completely oxidise the possible intermediates adsorbed on the surface, resulting in higher number of clean adsorption sites. Thus, this method could also be applied in real time operation of the possible air-cleaning device.

4. Conclusions

Organic-free acidic colloidal solution of TiO_2 anatase nanoparticles (denoted as AS in this article) was prepared from metatitanic acid using a novel environmentally friendly approach of TiO_2 nanoparticles precipitation with NaOH and peptization with HCl. For air treatment the high surface area of the catalyst is very important in order to enhance adsorption of VOCs on the catalyst surface before their degradation. AS was evaluated as a TiO_2–SiO_2 composite in the form of films for the total decomposition of toluene and formaldehyde as model VOCs. Low cost TiO_2–SiO_2 composite films made from acidic colloidal solution of TiO_2 anatase nanoparticles (AS) and mesoporous SiO_2 (SBA-15) with 100% loading (TiO_2:SiO_2 molar ratio 1:1) were prepared under simple procedure, low temperature and at ambient pressure. Moreover, the procedure involved no washing steps, hence practically zero waste was generated. The inertness of the material and its immobilization to a solid carrier further increase the sustainability of the synthesis method. These AS/SBA-15 films, immobilized by brush deposition on glass carriers, showed total decomposition of toluene and 91% decomposition of formaldehyde as model VOCs in gas phase, at room temperature under UVA irradiation in lab-made batch photoreactor. The trend of photocatalytic efficiency for decomposition of formaldehyde was AS/SBA-15 > P25 > PC500 > AS. The adsorption capability of the AS/SBA-15 was higher in comparison to its pure TiO_2 analogues (AS, P25, PC500) in case of toluene. Turnover frequency (TOF) of the AS/SBA-15 was approximately six times higher in comparison to its pure TiO_2 analogue AS for toluene and formaldehyde. Our results indicate that the increase in photocatalytic activity of the AS/SBA-15 sample is a combination of quantum size effect, due to reduced size of the nanocrystals, decreased number of crystal defects and enhanced adsorption of the pollutants due to the mesoporous nature of the SBA-15 support. Since real indoor air is a mixture of many pollutants, it is important to design a photocatalyst that addresses as many of them in the highest decomposition efficiency possible. The two contaminants used in this study (toluene and formaldehyde) are being considered as surrogates for two of the six major classes (aromatic, aldehyde, alkane, ketone, alcohol, and chlorocarbon) of indoor air contaminants [99], and therefore represent a good choice for testing the efficiency of newly synthesized photocatalysts.

The photocatalytic experiments were performed in a photocatalytic batch reactor with model VOC circulation and glass as a carrier. Further work and efforts, already in progress, are therefore to be oriented towards a continuous one-pass gas flow reactor with glass fibre filter based on quartz textile as a carrier (to mimic the air flow in the built-in filter in air cleaning devices). The advantage of the textile based on quartz fiberglass as a carrier when compared to glass carrier is in low content of sodium and shape flexibility. The long-term stability of the material is to be studied to evaluate the feasibility and sustainability of its use on a larger scale as a built-in filter in air cleaning devices for public buildings.

Acknowledgement

The authors gratefully acknowledge the financial support of the Slovenian Research Agency (ARRS) through PhD grant (A. Suligoj), Programs P1–0021, P2-0377 and project L1-4290.

References

[1] X. Pan, M.-Q. Yang, X. Fu, N. Zhang, Y.-J. Xu, Defective TiO_2 with oxygen vacancies: synthesis, properties and photocatalytic applications, Nanoscale 5 (2013) 3601–3614, http://dx.doi.org/10.1039/c3nr00476g.
[2] J.Z. Bloh, R. Dillert, D.W. Bahnemann, Designing optimal metal-doped photocatalysts: correlation between photocatalytic activity, doping ratio, and particle size, J. Phys. Chem. C 116 (2012) 25558–25562, http://dx.doi.org/10.1021/jp307313z.
[3] R. Marschall, L. Wang, Non-metal doping of transition metal oxides for visible-light photocatalysis, Catal. Today 225 (2014) 111–135, http://dx.doi.org/10.1016/j.cattod.2013.10.088.
[4] J. Chang, E.R. Waclawik, Colloidal semiconductor nanocrystals: controlled synthesis and surface chemistry in organic media, RSC Adv. 4 (2014) 23505, http://dx.doi.org/10.1039/c4ra02684e.
[5] T. Liu, F. Li, X. Li, TiO_2 hydrosols with high activity for photocatalytic degradation of formaldehyde in a gaseous phase, J. Hazard. Mater. 152 (2008) 347–355, http://dx.doi.org/10.1016/j.jhazmat.2007.07.003.
[6] X. Wang, F. Li, Y. Hao, S. Liu, M. Yang, TiO_2/SBA-15 composites prepared using H_2TiO_3 by hydrothermal method and its photocatalytic activity, Mater. Lett. 99 (2013) 38–41, http://dx.doi.org/10.1016/j.matlet.2013.02.060.
[7] Y. Zhang, Z.-R. Tang, X. Fu, Y.-J. Xu, TiO_2-graphene nanocomposites for gas-phase photocatalytic degradation of volatile aromatic pollutant: is TiO_2-graphene truly different from other TiO 2-carbon composite materials? ACS Nano 4 (2010) 7303–7314, http://dx.doi.org/10.1021/nn1024219.
[8] M.-Q. Yang, N. Zhang, M. Pagliaro, Y.-J. Xu, Artificial photosynthesis over graphene-semiconductor composites. Are we getting better? Chem. Soc. Rev. 43 (2014) 8240–8254, http://dx.doi.org/10.1039/C4CS00213J.
[9] N. Zhang, M.-Q. Yang, S. Liu, Y. Sun, Y.-J. Xu, Waltzing with the versatile platform of graphene to synthesize composite photocatalysts, Chem. Rev. 115 (2015) 10307–10377, http://dx.doi.org/10.1021/acs.chemrev.5b00267.

[10] N. Zhang, Y. Zhang, Y.-J. Xu, Recent progress on graphene-based photocatalysts: current status and future perspectives, Nanoscale 4 (2012) 5792, http://dx.doi.org/10.1039/c2nr31480k.
[11] S. Liu, Z.-R. Tang, Y. Sun, J.C. Colmenares, Y.-J. Xu, One-dimension-based spatially ordered architectures for solar energy conversion, Chem. Soc. Rev. 44 (2015) 5053–5075, http://dx.doi.org/10.1039/c4cs00408f.
[12] Z. Liu, X. Zhang, T. Murakami, A. Fujishima, Sol–gel SiO_2/TiO_2 bilayer films with self-cleaning and antireflection properties, Sol. Energy Mater. Sol. Cells 92 (2008) 1434–1438, http://dx.doi.org/10.1016/j.solmat.2008.06.005.
[13] L. Miao, L.F. Su, S. Tanemura, C.A.J. Fisher, L.L. Zhao, Q. Liang, et al., Cost-effective nanoporous SiO_2–TiO_2 coatings on glass substrates with antireflective and self-cleaning properties, Appl. Energy 112 (2013) 1198–1205, http://dx.doi.org/10.1016/j.apenergy.2013.03.043.
[14] S.R. Patil, B.H. Hameed, A.S. Škapin, U. Lavrenčič Štangar, Alternate coating and porosity as dependent factors for the photocatalytic activity of sol–gel derived TiO_2 films, Chem. Eng. J. 174 (2011) 190–198, http://dx.doi.org/10.1016/j.cej.2011.08.074.
[15] J. Taranto, D. Frochot, P. Pichat, Photocatalytic treatment of air: comparison of various TiO_2, coating methods, and supports using methanol or *n*-octane as test pollutant, Ind. Eng. Chem. Res. 48 (2009) 6229–6236 (accessed 17.03.14) http://pubs.acs.org/doi/abs/10.1021/ie900014f.
[16] B. Erdural, U. Bolukbasi, G. Karakas, Photocatalytic antibacterial activity of TiO_2–SiO_2 thin films: the effect of composition on cell adhesion and antibacterial activity, J. Photochem. Photobiol. A Chem. 283 (2014) 29–37, http://dx.doi.org/10.1016/j.jphotochem.2014.03.016.
[17] S.B. Kim, W.S. Cha, S.C. Hong, Photocatalytic degradation of gas-phase methanol and toluene using thin-film TiO_2 photocatalyst II. Kinetic study for the effect of initial concentration and photon flux, J. Ind. Eng. Chem. 8 (2002) 162–167.
[18] Y. Farhang Ghoje Biglu, E. Taheri-Nassaj, Investigation of phase separation of nano-crystalline anatase from TiO_2–SiO_2 thin film, Ceram. Int. 39 (2013) 2511–2518, http://dx.doi.org/10.1016/j.ceramint.2012.09.010.
[19] S.Z.Z. Chen, P.Y.Y. Zhang, W.P.P. Zhu, L. Chen, S.M.M. Xu, Deactivation of TiO_2 photocatalytic films loaded on aluminium: XPS and AFM analyses, Appl. Surf. Sci. 252 (2006) 7532–7538, http://dx.doi.org/10.1016/j.apsusc.2005.09.023.
[20] M. Addamo, V. Augugliaro, A. Di Paola, E. García-López, V. Loddo, G. Marcì, et al., Photocatalytic thin films of TiO_2 formed by a sol–gel process using titanium tetraisopropoxide as the precursor, Thin Solid Films 516 (2008) 3802–3807, http://dx.doi.org/10.1016/j.tsf.2007.06.139.
[21] J. Wang, C. Lu, J. Xiong, Self-cleaning and depollution of fiber reinforced cement materials modified by neutral TiO_2/SiO_2 hydrosol photoactive coatings, Appl. Surf. Sci. 298 (2014) 19–25, http://dx.doi.org/10.1016/j.apsusc.2013.12.171.
[22] P. Novotna, J. Krýsa, J. Maixner, P. Kluson, P. Novak, Photocatalytic activity of sol–gel TiO_2 thin films deposited on soda lime glass and soda lime glass precoated with a SiO_2 layer, Surf. Coat. Technol. 204 (2010) 2570–2575, http://dx.doi.org/10.1016/j.surfcoat.2010.01.043.
[23] Y. Situ, T. Huang, Y. Chen, W. Huang, H. Huang, Polymerization-induced phase separation in the preparation of macroporous TiO_2/SiO_2 thin films, Ceram. Int. 40 (2014) 919–927, http://dx.doi.org/10.1016/j.ceramint.2013.06.087.
[24] H.S. Jung, H. Kim, Origin of low photocatalytic activity of rutile TiO_2, Electron. Mater. Lett. 5 (2009) 73–76, http://dx.doi.org/10.3365/eml.2009.06.073.
[25] Z. Han, V.W.C. Chang, L. Zhang, M.S. Tse, O.K. Tan, L.M. Hildemann, Preparation of TiO_2-coated polyester fiber filter by spray-coating and its photocatalytic degradation of gaseous formaldehyde, Aerosol. Air Qual. Res. 12 (2012) 1327–1335, http://dx.doi.org/10.4209/aaqr.2012.05.0114.
[26] O. Carp, C.L. Huisman, A. Reller, Photoinduced reactivity of titanium dioxide, Prog. Solid State Chem. 32 (2004) 33–177, http://dx.doi.org/10.1016/j.progsolidstchem.2004.08.001.
[27] A.Y. Shan, T.I.M. Ghazi, S.A. Rashid, Immobilisation of titanium dioxide onto supporting materials in heterogeneous photocatalysis: a review, Appl. Catal. A Gen. 389 (2010) 1–8, http://dx.doi.org/10.1016/j.apcata.2010.08.053.
[28] U. Černigoj, U. Lavrenčič Štangar, P. Trebše, Photocatalytically active TiO_2 thin films produced by surfactant-assisted sol–gel processing, Thin Solid Films 495 (2006) 327–332, http://dx.doi.org/10.1016/j.tsf.2005.08.240.
[29] U. Černigoj, U. Lavrenčič Štangar, P. Trebše, Degradation of neonicotinoid insecticides by different advanced oxidation processes and studying the effect of ozone on TiO_2 photocatalysis, Appl. Catal. B Environ. 75 (2007) 229–238, http://dx.doi.org/10.1016/j.apcatb.2007.04.014.
[30] M. Tasbihi, U. Lavrenčič Štangar, U. Černigoj, K. Kogej, Low-temperature synthesis and characterization of anatase TiO_2 powders from inorganic precursors, Photochem. Photobiol. Sci. 8 (2009) 719, http://dx.doi.org/10.1039/b817472e.
[31] U. Černigoj, M. Kete, U. Lavrenčič Štangar, Development of a fluorescence-based method for evaluation of self-cleaning properties of photocatalytic layers, Catal. Today 151 (2010) 46–52, http://dx.doi.org/10.1016/j.cattod.2010.03.043.
[32] K. Drew, G. Girishkumar, K. Vinodgopal, P.V. Kamat, Boosting Fuel Cell Performance with a semiconductor photocatalyst: TiO 2 /Pt-Ru hybrid catalyst for methanol oxidation, J. Phys. Chem. B 109 (2005) 11851–11857, http://dx.doi.org/10.1021/jp051073d.
[33] U. Lavrenčič Štangar, U. Černigoj, P. Trebše, K. Maver, S. Gross, Photocatalytic TiO_2 coatings: effect of substrate and template, Monatsh. Chem. 64 (2006) 7–655, http://dx.doi.org/10.1007/s00706-006-0443-y.
[34] J. Zita, J. Krýsa, A. Mills, Correlation of oxidative and reductive dye bleaching on TiO_2 photocatalyst films, J. Photochem. Photobiol. A Chem. 203 (2009) 119–124, http://dx.doi.org/10.1016/j.jphotochem.2008.12.029.
[35] P. Novotná, J. Zita, J. Krýsa, V. Kalousek, J. Rathouský, Two-component transparent TiO_2/SiO_2 and TiO_2/PDMS films as efficient photocatalysts for environmental cleaning, Appl. Catal. B Environ. 79 (2008) 179–185, http://dx.doi.org/10.1016/j.apcatb.2007.10.012.
[36] X. Gao, I.E. Wachs, Titania-silica as catalysts: molecular structural characteristics and physico–chemical properties, Catal. Today 51 (1999) 233–254, http://dx.doi.org/10.1016/s0920-5861(99) 48-6.
[37] J. Su, X. Zou, J.-S. Chen, Self-modification of titanium dioxide materials by Ti^{3+} and/or oxygen vacancies: new insights into defect chemistry of metal oxides, RSC Adv. 4 (2014) 13979, http://dx.doi.org/10.1039/c3ra47757f.
[38] S. Rodrigues, K.T. Ranjit, S. Uma, I.N. Martyanov, K.J. Klabunde, Single-step synthesis of a highly active visible-light photocatalyst for oxidation of a common indoor air pollutant: acetaldehyde, Adv. Mater. 17 (2005) 2467–2471, http://dx.doi.org/10.1002/adma.200402064.
[39] M. Tasbihi, U. Lavrenčič Štangar, A.S. Škapin, A. Ristić, V. Kaučič, N. Novak Tušar, Titania-containing mesoporous silica powders: structural properties and photocatalytic activity towards isopropanol degradation, J. Photochem. Photobiol. A Chem. 216 (2010) 167–178, http://dx.doi.org/10.1016/j.jphotochem.2010.07.011.
[40] M. Tasbihi, U. Lavrenčič Štangar, U. Černigoj, J. Jirkovský, S. Bakardijeva, N. Novak Tušar, Photocatalytic oxidation of gaseous toluene on titania/mesoporous silica powders in a fluidized-bed reactor, Catal. Today 161 (2011) 181–188, http://dx.doi.org/10.1016/j.cattod.2010.08.015.
[41] M.-J. López-Muñoz, R. van Grieken, J. Aguado, J. Marugán, Role of the support on the activity of silica-supported TiO_2 photocatalysts: structure of the TiO_2/SBA-15 photocatalysts, Catal. Today 101 (2005) 307–314, http://dx.doi.org/10.1016/j.cattod.2005.03.017.
[42] Y. Kuwahara, H. Yamashita, Efficient photocatalytic degradation of organics diluted in water and air using TiO_2 designed with zeolites and mesoporous silica materials, J. Mater. Chem. 21 (2011) 2407–2416, http://dx.doi.org/10.1039/C0JM02741C.
[43] X. Qian, K. Fuku, Y. Kuwahara, T. Kamegawa, K. Mori, H. Yamashita, Design and functionalization of photocatalytic systems within mesoporous silica, ChemSusChem 7 (2014) 1528–1536, http://dx.doi.org/10.1002/cssc.201400111.
[44] D. Zhao, J. Feng, Q. Huo, N. Melosh, G. Fredrickson, B. Chmelka, et al., Triblock copolymer syntheses of mesoporous silica with periodic 50–300 angstrom pores, Science 279 (1998) 548–552, http://dx.doi.org/10.1126/science.279.5350.548 (80-.).
[45] F. Zhang, Y. Zheng, Y. Cao, C. Chen, Y. Zhan, X. Lin, et al., Ordered mesoporous Ag–TiO_2–KIT-6 heterostructure: synthesis, characterization and photocatalysis, J. Mater. Chem. 19 (2009) 2771, http://dx.doi.org/10.1039/b818495j.
[46] M. Signoretto, E. Ghedini, V. Trevisan, C.L. Bianchi, M. Ongaro, G. Cruciani, TiO_2–MCM-41 for the photocatalytic abatement of NOx in gas phase, Appl. Catal. B Environ. 95 (2010) 130–136, http://dx.doi.org/10.1016/j.apcatb.2009.12.019.
[47] J. Yang, J. Zhang, L. Zhu, S. Chen, Y. Zhang, Y. Tang, et al., Synthesis of nano titania particles embedded in mesoporous SBA-15: characterization and photocatalytic activity, J. Hazard. Mater. 137 (2006) 952–958, http://dx.doi.org/10.1016/j.jhazmat.2006.03.017.
[48] H. Lachheb, O. Ahmed, A. Houas, J.P. Nogier, Photocatalytic activity of TiO_2–SBA-15 under UV and visible light, J. Photochem. Photobiol. A Chem. 226 (2011) 1–8, http://dx.doi.org/10.1016/j.jphotochem.2011.09.017.
[49] W. Yan, S.M. Mahurin, S.H. Overbury, S. Dai, Nonhydrolytic layer-by-layer surface sol–gel modification of powdered mesoporous silica materials with TiO_2, Chem. Mater. 17 (2005) 1923–1925, http://dx.doi.org/10.1021/cm048118s.
[50] K. De Witte, A.M. Busuioc, V. Meynen, M. Mertens, N. Bilba, G. Van Tendeloo, et al., Influence of the synthesis parameters of TiO_2-SBA-15 materials on the adsorption and photodegradation of rhodamine-6G, Microporous Mesoporous Mater 110 (2008) 100–110, http://dx.doi.org/10.1016/j.micromeso.2007.09.035.
[51] W. Dong, Y. Sun, C.W. Lee, W. Hua, X. Lu, Y. Shi, et al., Controllable and repeatable synthesis of thermally stable anatase nanocrystal-silica composites with highly ordered hexagonal mesostructures, J. Am. Chem. Soc. 129 (2007) 13894–13904, http://dx.doi.org/10.1021/ja073804o.
[52] H. Ding, H. Sun, Y. Shan, Preparation and characterization of mesoporous SBA-15 supported dye-sensitized TiO_2 photocatalyst, J. Photochem. Photobiol. A Chem. 169 (2005) 101–107, http://dx.doi.org/10.1016/j.jphotochem.2004.04.015.
[53] R. van Grieken, J. Aguado, M.J. López-Muñoz, J. Marugán, Synthesis of size-controlled silica-supported TiO_2 photocatalysts, J. Photochem. Photobiol. A Chem. 148 (2002) 315–322, http://dx.doi.org/10.1016/S1010-6030(02) 00058-8.
[54] A.M. Busuioc, V. Meynen, E. Beyers, M. Mertens, P. Cool, N. Bilba, et al., Structural features and photocatalytic behaviour of titania deposited within the pores of SBA-15, Appl. Catal. A Gen. 312 (2006) 153–164, http://dx.doi.org/10.1016/j.apcata.2006.06.043.
[55] K. De Witte, V. Meynen, M. Mertens, O.I. Lebedev, G. Van Tendeloo, A. Sepúlveda-Escribano, et al., Multi-step loading of titania on mesoporous silica: influence of the morphology and the porosity on the catalytic

degradation of aqueous pollutants and VOCs, Appl. Catal. B Environ. 84 (2008) 125–132, http://dx.doi.org/10.1016/j.apcatb.2008.03.015.
[56] E. Beyers, E. Biermans, S. Ribbens, K. De Witte, M. Mertens, V. Meynen, et al., Combined TiO_2/SiO_2 mesoporous photocatalysts with location and phase controllable TiO_2 nanoparticles, Appl. Catal. B Environ. 88 (2009) 515–524, http://dx.doi.org/10.1016/j.apcatb.2008.10.009.
[57] C. Kang, L. Jing, T. Guo, H. Cui, J. Zhou, H. Fu, Mesoporous SiO_2-modified nanocrystalline TiO_2 with high anatase thermal stability and large surface area as efficient photocatalyst, J. Phys. Chem. C 113 (2009) 1006–1013, http://dx.doi.org/10.1021/jp807552u.
[58] W.A. Adams, M.G. Bakker, T. Macias, I.A. Jefcoat, Synthesis and characterization of mesoporous silica films encapsulating titanium dioxide particles; photodegradation of 2,4-dichlorophenol, J. Hazard. Mater. 112 (2004) 253–259, http://dx.doi.org/10.1016/j.jhazmat.2004.05.015.
[59] D.M. Tobaldi, A. Tucci, A.S. Škapin, L. Esposito, Effects of SiO_2 addition on TiO_2 crystal structure and photocatalytic activity, J. Eur. Ceram. Soc. 30 (2010) 2481–2490, http://dx.doi.org/10.1016/j.jeurceramsoc.2010.05.014.
[60] A. Tuel, L.G. Hubert-Pfalzgraf, Nanometric monodispersed titanium oxide particles on mesoporous silica: synthesis, characterization, and catalytic activity in oxidation reactions in the liquid phase, J. Catal. 217 (2003) 343–353, http://dx.doi.org/10.1016/s0021-9517(03) 78-2.
[61] W. Yan, B. Chen, S.M. Mahurin, E.W. Hagaman, S. Dai, S.H. Overbury, Surface sol-gel modification of mesoporous silica materials with TiO_2 for the assembly of ultrasmall gold nanoparticles, J. Phys. Chem. B 108 (2004) 2793–2796, http://dx.doi.org/10.1021/jp037713z.
[62] M. Alvaro, C. Aprile, M. Benitez, E. Carbonell, H. García, Photocatalytic activity of structured mesoporous TiO_2 materials, J. Phys. Chem. B 110 (2006) 6661–6665, http://dx.doi.org/10.1021/jp0573240.
[63] S. Perathoner, P. Lanzafame, R. Passalacqua, G. Centi, R. Schlögl, D.S. Su, Use of mesoporous SBA-15 for nanostructuring titania for photocatalytic applications, Microporous Mesoporous Mater. 90 (2006) 347–361, http://dx.doi.org/10.1016/j.micromeso.2005.10.024.
[64] H.G. Yang, C.H. Sun, S.Z. Qiao, J. Zou, G. Liu, S.C. Smith, et al., Anatase TiO_2 single crystals with a large percentage of reactive facets, Nature 453 (2008) 638–641, http://dx.doi.org/10.1038/nature06964.
[65] W.-J. Ong, L.-L. Tan, S.-P. Chai, S.-T. Yong, A.R. Mohamed, Facet-dependent photocatalytic properties of tio2 -based composites for energy conversion and environmental remediation, ChemSusChem 7 (2014) 690–719, http://dx.doi.org/10.1002/cssc.201300924.
[66] M. Tasbihi, M. Kete, A.M. Raichur, U. Lavrenčič Štangar, N. Novak Tušar, Photocatalytic degradation of gaseous toluene by using immobilized titania/silica on aluminum sheets, Environ. Sci. Pollut. Res. 19 (2012) 3735–3742, http://dx.doi.org/10.1007/s11356-012-0864-6.
[67] A. Šuligoj, U.L. Štangar, N.N. Tušar, Photocatalytic air-cleaning using TiO_2 nanoparticles in porous silica substrate, Chem. Pap. 68 (2014) 1265–1272, http://dx.doi.org/10.2478/s11696-014-0553-7.
[68] D. Verhovšek, N. Veronovski, U. Lavrenčič Štangar, M. Kete, K. Žagar, M. Čeh, The synthesis of anatase nanoparticles and the preparation of photocatalytically active coatings based on wet chemical methods for self-cleaning applications, Int. J. Photoenergy 2012 (2012), http://dx.doi.org/10.1155/2012/329796.
[69] R.A. Spurr, H. Myers, Quantitative analysis of anatase-rutile mixtures with an X-Ray diffractometer, Anal. Chem. 29 (1957) 760–762, http://dx.doi.org/10.1021/ac60125a006.
[70] D.A.H. Hanaor, C.C. Sorrell, Review of the anatase to rutile phase transformation, J. Mater. Sci. 46 (2011) 855–874, http://dx.doi.org/10.1007/s10853-010-5113-0.
[71] S. Brunauer, P.H. Emmett, E. Teller, Adsorption of gases in multimolecular layers, J. Am. Chem. Soc. 60 (1938) 309–319, http://dx.doi.org/10.1021/ja01269a023.
[72] K.S.W. Sing, D.H. Everett, R.A.W. Haul, L. Moscou, R.A. Pierotti, J. Rouquerol, et al., Reporting physisorption data for gas/solid systems with special reference to the determination of surface area and porosity, Pure Appl. Chem. 57 (1985) 603–619, http://dx.doi.org/10.1351/pac198557040603.
[73] E.P. Barrett, L.G. Joyner, P.P. Halenda, The determination of pore volume and area distributions in porous substances. I. computations from nitrogen isotherms, J. Am. Chem. Soc. 73 (1951) 373–380, http://dx.doi.org/10.1021/ja01145a126.
[74] P. Thanigainathan, C. Paramasivan, Growth and characterization of optically confined particulate films of anatase TiO_2, Int. Nano Lett. 2 (2012) 34, http://dx.doi.org/10.1186/2228-5326-2-34.
[75] S. Kozuch, J.M.L. Martin, Turning over definitions in catalytic cycles, ACS Catal. 2 (2012) 2787–2794, http://dx.doi.org/10.1021/cs3005264.
[76] L.P. Childs, D.F. Ollis, Is photocatalysis catalytic? J. Catal. 66 (1980) 383–390, http://dx.doi.org/10.1016/0021-9517(80) 90041-x.
[77] B. Ohtani, O.O. Prieto-Mahaney, D. Li, R. Abe, What is degussa (Evonik) P25? Crystalline composition analysis, reconstruction from isolated pure particles and photocatalytic activity test, J. Photochem. Photobiol. A Chem. 216 (2010) 179–182, http://dx.doi.org/10.1016/j.jphotochem.2010.07.024.
[78] A. Lemaire, J.C. Rooke, L.H. Chen, B.L. Su, Direct observation of macrostructure formation of hierarchically structured meso-macroporous aluminosilicates with 3D interconnectivity by optical microscope, Langmuir 27 (2011) 3030–3043, http://dx.doi.org/10.1021/la104679h.
[79] M. Kruk, M. Jaroniec, Gas adsorption characterization of ordered organic–inorganic nanocomposite materials, Chem. Mater. 13 (2001) 3169–3183, http://dx.doi.org/10.1021/cm0101069.
[80] W.W. Lukens, P. Schmidt-Winkel, D. Zhao, J. Feng, G.D. Stucky, Evaluating pore sizes in mesoporous materials: a simplified standard adsorption method and a simplified Broekhoff-de Boer method, Langmuir 15 (1999) 5403–5409, http://dx.doi.org/10.1021/la990209u.
[81] P.T. Tanev, L.T. Vlaev, An attempt at a more precise evaluation of the approach to mesopore size distribution calculations depending on the degree of pore blocking, J. Colloid Interface Sci. 160 (1993) 110–116, http://dx.doi.org/10.1006/jcis.1993.1374.
[82] X. Mao, X. Lang, Z. Wang, Q. Hao, B. Wen, Z. Ren, et al., Band-Gap States of TiO_2 (1 1 0): major contribution from surface defects, J. Phys. Chem. Lett. 4 (2013) 3839–3844, http://dx.doi.org/10.1021/jz402053p.
[83] M.M. Khan, S.A. Ansari, D. Pradhan, M.O. Ansari, D.H. Han, J. Lee, et al., Band gap engineered TiO_2 nanoparticles for visible light induced photoelectrochemical and photocatalytic studies, J. Mater. Chem. A 2 (2014) 637–644, http://dx.doi.org/10.1039/c3ta14052k.
[84] B. Choudhury, A. Choudhury, Oxygen defect dependent variation of band gap, Urbach energy and luminescence property of anatase, anatase–rutile mixed phase and of rutile phases of TiO_2 nanoparticles, Phys. E Low-Dimensional Syst. Nanostruct. 56 (2014) 364–371, http://dx.doi.org/10.1016/j.physe.2013.10.014.
[85] H. Lin, C.P. Huang, W. Li, C. Ni, Size dependency of nanocrystalline TiO_2 on its optical property and photocatalytic reactivity exemplified by 2-chlorophenol, Appl. Catal. B Environ. 68 (2006) 1–11, http://dx.doi.org/10.1016/j.apcatb.2006.07.018.
[86] A. Welte, C. Waldauf, C. Brabec, P.J. Wellmann, Application of optical absorbance for the investigation of electronic and structural properties of sol–gel processed TiO_2 films, Thin Solid Films 516 (2008) 7256–7259, http://dx.doi.org/10.1016/j.tsf.2007.12.025.
[87] T. Ohno, S. Tagawa, H. Itoh, H. Suzuki, T. Matsuda, Size effect of TiO_2–SiO_2 nano-hybrid particle, Mater. Chem. Phys. 113 (2009) 119–123, http://dx.doi.org/10.1016/j.matchemphys.2008.07.034.
[88] X. Zhang, F. Zhang, K.-Y. Chan, Synthesis of titania–silica mixed oxide mesoporous materials, characterization and photocatalytic properties, Appl. Catal. A Gen. 284 (2005) 193–198, http://dx.doi.org/10.1016/j.apcata.2005.01.037.
[89] Y.J. Acosta-Silva, R. Nava, V. Hernández-Morales, S.A. Macías-Sánchez, M.L.L. Gómez-Herrera, B. Pawelec, Methylene blue photodegradation over titania-decorated SBA-15, Appl. Catal. B Environ. 110 (2011) 108–117, http://dx.doi.org/10.1016/j.apcatb.2011.08.032.
[90] G. Marcì, V. Augugliaro, M.J. López-Muñoz, C. Martín, L. Palmisano, V. Rives, et al., Preparation characterization and photocatalytic activity of polycrystalline ZnO/TiO_2 systems 2. surface, bulk characterization, and 4-nitrophenol photodegradation in liquid–solid regime, J. Phys. Chem. B. 105 (2001) 1033–1040, http://dx.doi.org/10.1021/jp003173j.
[91] L. Cao, Photocatalytic oxidation of toluene on nanoscale TiO_2 catalysts: studies of deactivation and regeneration, J. Catal. 196 (2000) 253–261, http://dx.doi.org/10.1006/jcat.2000.3050.
[92] N. Quici, M.L. Vera, H. Choi, G.L. Puma, D.D. Dionysiou, M.I. Litter, et al., Effect of key parameters on the photocatalytic oxidation of toluene at low concentrations in air under 254 + 185 nm UV irradiation, Appl. Catal. B Environ. 95 (2010) 312–319, http://dx.doi.org/10.1016/j.apcatb.2010.01.009.
[93] M. Nagao, Y. Suda, Adsorption of benzene, toluene, and chlorobenzene on titanium dioxide, Langmuir 5 (1989) 42–47, http://dx.doi.org/10.1021/la00085a009.
[94] T. Daubert, R. Danner, Physical and Thermodynamic Properties of Pure Chemicals: Data Compilation, Part 1, Taylor & Francis, Washington, DC, 1989.
[95] Y. Liao, C. Xie, Y. Liu, H. Chen, H. Li, J. Wu, Comparison on photocatalytic degradation of gaseous formaldehyde by TiO_2, ZnO and their composite, Ceram. Int. 38 (2012) 4437–4444, http://dx.doi.org/10.1016/j.ceramint.2012.03.016.
[96] Y. Zhang, G. Xiong, N. Yao, W. Yang, X. Fu, Preparation of titania-based catalysts for formaldehyde photocatalytic oxidation from $TiCl_4$ by the sol–gel method, Catal. Today 68 (2001) 89–95, http://dx.doi.org/10.1016/S0920-5861(01) 00295-4.
[97] C. He, W. Chen, K. Han, B. Guo, J. Pei, J.S. Zhang, Evaluation of filter media performance: correlation between high and low challenge concentration tests for toluene and formaldehyde (ASHRAE RP-1557), HVAC R Res. 20 (2014) 508–521, http://dx.doi.org/10.1080/10789669.2014.907096.
[98] I.E. Wachs, S.P. Phivilay, C.A. Roberts, Reporting of reactivity for heterogeneous photocatalysis, ACS Catal. 3 (2013) 2606–2611, http://dx.doi.org/10.1021/cs4005979.
[99] T.N. Obee, R.T. Brown, TiO_2 Photocatalysis for indoor air applications: effects of humidity and trace contaminant levels on the oxidation rates of formaldehyde, toluene, and 1,3-butadiene, Environ. Sci. Technol. 29 (1995) 1223–1231, http://dx.doi.org/10.1021/es00005a013.